THE ASTROPHYSICAL JOURNAL, 373:146–157, 1991 May 20

RELATIVISTIC ELECTRON POPULATIONS IN CASSIOPEIA A

M. ANDERSON, L. RUDNICK, AND P. LEPPIK
Department of Astronomy, University of Minnesota, 116 Church Street SE, Minneapolis, MN 55455
R. PERLEY
National Radio Astronomy Observatory/Array Operations Center, P.O. Box O, Socorro, NM 87801
AND
R. BRAUN[1]
Netherlands Foundation for Radio Astronomy, Postbus 2, NL-7990AA Dwingeloo, Netherlands
Received 1990 July 6; accepted 1990 November 1

ABSTRACT

Spectral index variations are observed in the radio brightness distribution in the supernova remnant Cassiopeia A, between observing wavelengths of $\lambda 20$ cm and $\lambda 6$ cm. Reliable variations are seen over a range of -0.64 to -0.92, with steeper spectra typically associated with compact features such as the "bow shocks" and flatter spectra with the bright radio ring. The spatial scales over which significant variations are detected range from $\sim 11''$ to greater than $80''$. The importance of these results is that they indicate a direct link between the dynamics of the remnant and the relativistic particle energy distributions. Building on previously suggested dynamical pictures, we suggest that the bow shocks are caused by moderately dense clumps of ejecta newly encountering the shocked ISM. We find that models based on first-order Fermi acceleration in the test particle limit are unable to explain, concurrently, the steep spectral indices and the high synchrotron emissivities observed in Cas A. Thus, consideration of other types of processes, such as acceleration in cosmic ray–mediated shocks and turbulent acceleration with secularly increasing B fields, is required.

Subject headings: nebulae: individual (Cas A) — nebulae: supernova remnants — particle acceleration — radiation mechanisms — radio sources: spectra

1. INTRODUCTION

Supernova remnants are widely regarded as the primary acceleration site for galactic cosmic rays. Shelllike supernova remnants such as Cassiopeia A (Cas A) without a current central energy source, are expected to accelerate particles through shock and/or turbulent Fermi mechanisms. The spectral index of the radio synchrotron radiation should be an excellent probe of the electron energy distributions, but this line of investigation has not been very productive so far.

While radio supernova remnants as a class of astrophysical objects exhibit a wide variety of overall spectral indices ($-0.3 < \alpha < -0.8$, where $S_\nu \propto \nu^\alpha$), individual remnants have generally shown very little, if any, internal variations in spectral index (e.g., Tycho's SNR is uniform to 5% in α; Klein et al. 1979). Indeed, it has been predicted that spatial variations in α are unlikely, given the short time scales on which particle acceleration is expected to occur in the remnant environment (Reynolds 1988a). Based on recent, high-quality radio maps of supernova remnant Cas A at 1.4 and 5.0 GHz with $1\farcs3$ resolution, we report evidence for significant spectral variations of order ± 0.15 in α about the overall value of -0.77 (Baars et al. 1977), opening the way for studying the conditions and mechanisms of the particle acceleration process.

Previously published studies of spectral index in Cas A have been conducted at low resolutions, where small spatial-scale variations in α are potentially smeared out. Rosenberg (1970) found some indication of variation in spectra between 1.4, 2.7, and 5.0 GHz at $\sim 25''$ resolution; however, given the large uncertainties in the measurements (± 0.15 to ± 0.20 in α), nothing definitive could be said. Spectral comparisons between observations at 81.5 and 1381 MHz by Woan & Duffett-Smith (1990) down to angular scales of $6''$ also indicate variations in spectral index across Cas A. They find that spectrally steep regions in the remnant tend to be found in compact features, while flatter regions are more spread out. These overall conclusions are in agreement with the work presented below. However, some of their spectral indices appear to come from regions of very low signal-to-noise, so the reliability is difficult to evaluate.

The spectrum of Cas A appears to be varying temporally as well as spatially. Dent, Aller, & Olsen (1974) reported a secular spectral flattening at a rate of $+0.00126$ in α per year. Scott & Chevalier (1975) modeled this flattening with a continuous acceleration of particles through scattering off regions of turbulent magnetic field which may be generated in the wakes of the fast-moving optical knots. A plot of spectral index versus diameter for a set of shell SNRs with well-established distances (Fig. 1, adapted from Green 1988) suggests that such flattening may be a common evolutionary trend in young shell SNRs, although, as Green points out, a given remnant will likely travel over only a fraction of this track during its lifetime.

For the sake of comparison, we have included in Figure 1 a point representing a typical compact bow shock feature in Cas A, and have indicated the spectral indices of the galactic synchrotron background, measured above and below the break in the spectrum which occurs at about 400 MHz. In this paper we will explore a variety of scenarios in which relativistic and subrelativistic electrons from the interstellar medium are injected into various shock structures in Cas A and subsequently accelerated via the first-order Fermi mechanism. We discuss the difficulties that first-order models have in explaining our observations and stress the need for detailed modeling

[1] Also National Radio Astronomy Observatory.

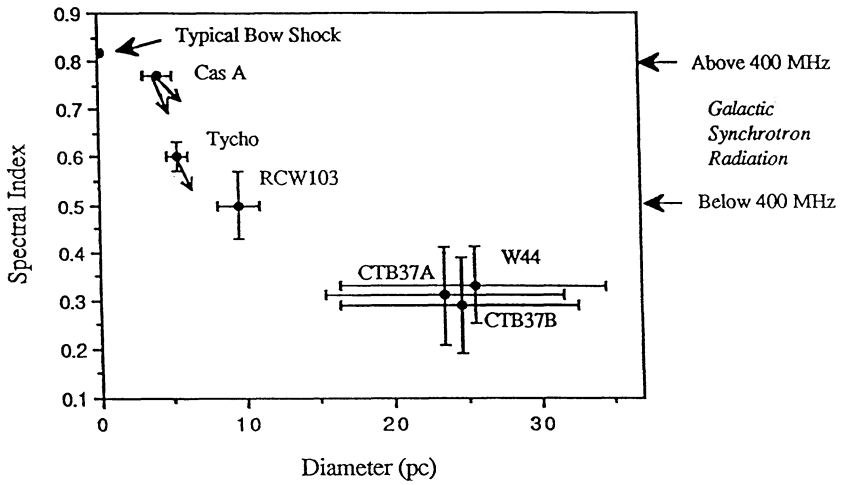

FIG. 1.—Plot of spectral index vs. size for shell SNRs with good distance estimates (adapted from Green 1988). Also included is a point indicating a typical bow shock in Cas A, as discussed in this paper, and arrows indicating the spectral indices of the galactic synchrotron radiation above and below the spectral break at around 400 MHz (Bridle 1967; Sironi 1974; Webster 1974). Arrows on Cas A and Tycho represent the current rate of observed spectral flattening, although these rates will likely diminish with time.

of cosmic ray–mediated shocks and other particle acceleration mechanisms in Cas A.

2. OBSERVATIONS

The spectral data presented here are based on observations made with the Very Large Array (VLA;[2] Thompson et al. 1980) in 1987. To increase aperture coverage, data were taken at several frequencies around the nominal frequencies of 1.4 and 4.8 GHz (L and C bands), and in a combination of the standard VLA configurations. Details of the observations are summarized in Table 1. This set of observations is part of a 10 year program to monitor changes in Cas A at high resolution. Five epochs of observations have been obtained to date—three with the VLA, and two with the Cambridge 5 km telescope. Another set of VLA observations was conducted in 1990.

2.1. *Calibration and Mapping*

Primary flux calibrations in all observing sessions were based on 3C48, with secondary calibrations from bootstrapped fluxes for 2352+495 and 3C138. Due to the size of the combined data bases (greater than 10^6 visibilities), data from each array were edited and self-calibrated individually. Each data set was divided by the Fourier transform of a model derived from the data themselves and from data on all longer baselines. Gain corrections were determined and applied to the original data. The data were then concatenated and mapped via the AIPS maximum entropy routine VTESS to produce the full synthesis images presented here. Although zero-spacing flux densities were not specified at either band, VTESS was able to reconstruct 97% of the total expected flux at L band (as given by the Baars' scale; Baars et al. 1977) and 95% at C band. The specified target rms residual levels were 0.04 mJy pixel^{-1} at both L and C, where each pixel is a square of dimension 0.″4. These noise values were determined in part by the rms measured in Stokes Q and U maps and in part to facilitate the convergence of VTESS. Both maps have been corrected for primary beam attenuation and convolved to 1.″3 to fix the resolution and to minimize errors due to motions of features within the source. The original maps (2048^2) were constructed on the Convex at the National Radio Astronomy Observatory in Socorro, NM. Subsequent maps were made on the Cray X-MP at the Minnesota Supercomputer Center to investigate the robustness of the low-brightness background reconstruction with various short UV-spacing cutoffs.

[2] The Very Large Array is a facility of the National Radio Astronomy Observatory, operated by Associated Universities, Inc., under contract with the National Science Foundation.

2.2. *Structures in Total Intensity*

Figure 2 shows the total intensity image of Cas A at 1.4 GHz in 1987. The structure of this remnant is complex and is distributed over a variety of spatial scales. A few major components are apparent. The most prominent is a *bright ring* of radio emission, at a radius of ~110″ (1.7 pc at a distance of 2.9 kpc). This bright ring is generally associated with a region of high magnetic field, amplified through Rayleigh-Taylor instabilities which develop at the contact surface between the comparatively dense supernova ejecta and the shock-heated interstellar medium as the remnant begins to decelerate (Gull 1975). The bright ring has an expansion age of 950 yr (Tuffs 1986), much longer than that of the fast-moving optical knots situated at a similar radius (300 yr; van den Bergh & Dodd 1970), indicating that a substantial deceleration of the radio-emitting ejecta has

TABLE 1

SUMMARY OF VLA OBSERVATIONS FOR EPOCH 1987 MAPS

VLA Configuration	Date	Frequencies (MHz)	Duration (hr)
		λ20 cm	
A	1987.6	1381, 1456, 1536, 1626	5.5
B	1987.9	1381, 1626	3.0
C	1988.2	1446, 1496	1.0
D	1987.4	1465, 1515	0.3
		λ6 cm	
B	1987.9	4640, 4970	4.5
C	1988.2	4816, 4823, 4866, 4873	1.0
D	1987.4	4835, 4885	0.5

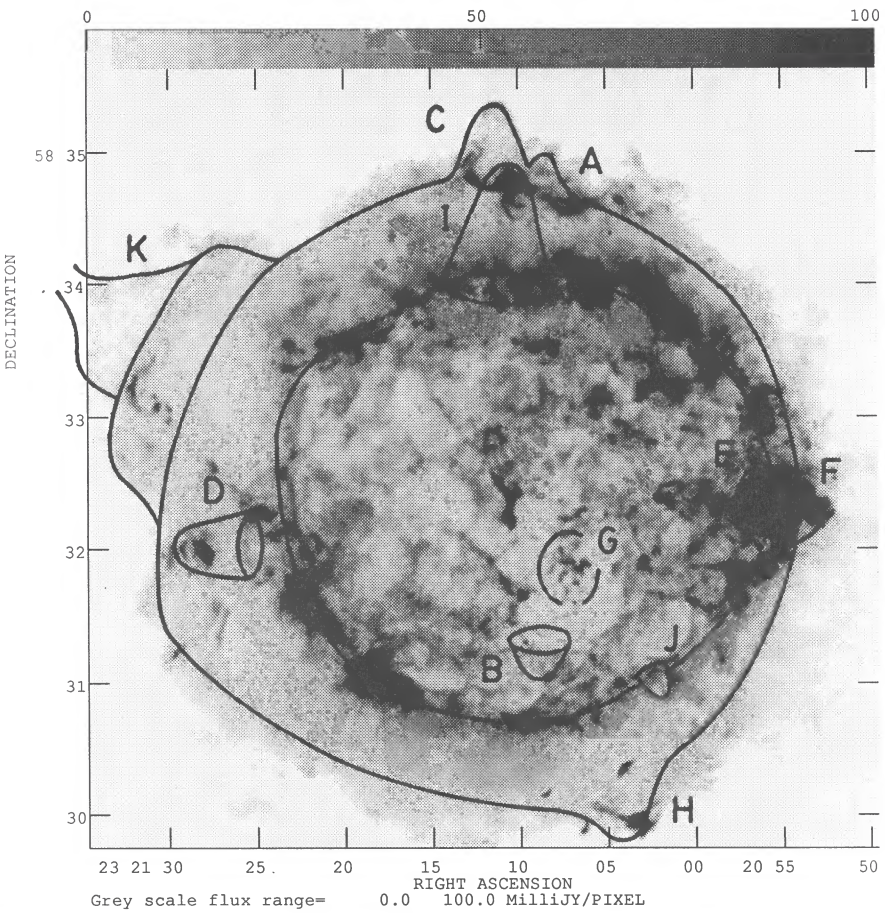

FIG. 2.—Gray-scale total intensity map of Cas A at $\lambda 20$ cm, epoch 1987. The beam size is 1".3. Overlaid are the main features discussed by BGP: the bright inner ring, the outer plateau, and the bow shocks.

already occurred. A limb-brightened shell of similar thickness and radius is found in X-ray observations (Fabian et al. 1980), fitted by Jansen et al. (1988), with a continuum temperature of 7.5×10^6 K. This material may have been heated by a reverse shock interior to the contact discontinuity, generated in the overall deceleration of the ejecta.

A *plateau*, or *outer shell*, of material is seen out to a radius of $\approx 140''$. Braun (1987) and Braun, Gull, & Perley (1987, hereafter BGP) identified this plateau with a shell of material from the back (larger) hemisphere of Cas A. Radial velocities of optical fast-moving knots (Minkowski 1959) indicate that the receding hemisphere of the shell is larger than the forward (Braun 1987), perhaps because of variations in the density of the external medium. The plateau also has a weak X-ray counterpart (Fabian et al. 1980) with temperature 3.3×10^7 K (Jansen et al. 1988). Others have suggested that this X-ray emission may arise from circumstellar material heated by the outer shock (e.g., Fabian et al. 1980). Average levels of the plateau in our images are approximately 2 mJy pixel^{-1} at 1.4 GHz and 1 mJy pixel^{-1} at 5.0 GHz. If we assume the missing flux due to unsampled short spacings (see § 3.1) is distributed uniformly across the plateau, these values underestimate the true brightnesses in the plateau by $\sim 9\%$ and 12%, respectively.

Evidence for a third, large-scale X-ray component, extending out to $r \geq 6'$, has been found by Stewart, Fabian, & Seward (1983). However, Mauche & Gorenstein (1989) have been able to model this halo with scattering of X-rays from the other components by interstellar grains.

A set of eleven paraboloidal features or *bow shocks* were identified by BGP (schematics overlaid on Fig. 2). Their morphologies, motions, and magnetic field configurations seem to indicate clumps of fast-moving ejecta which have penetrated the decelerated shell and are generating bow shocks in the material beyond the shells. If this interpretation is correct, these features may be sites of recently commenced particle acceleration. Our results and an interpretation of the spectra of these bow shocks will be discussed below.

The remnant is also covered by a network of faint *filamentation*, the nature of which is still unclear. These may be actual filaments of compressed gas, condensed under some type of cooling or dynamical instability (e.g., Reynolds 1988b), or perhaps they are features of numerous intersecting shock waves, propagating through the remnant (P. Woodward 1988, private communication). Unfortunately, these filaments are too faint for reliable spectral measurements, given our current limitations. With new observations and improved spatial filtering techniques we hope to extend our studies to these fainter features.

3. SPECTRAL INDEX MEASUREMENTS

Figure 3 shows the distribution of spectral index in Cas A, determined between points at 1.4 and 4.8 GHz from the epoch 1987 data. The map has been clipped to contain only points

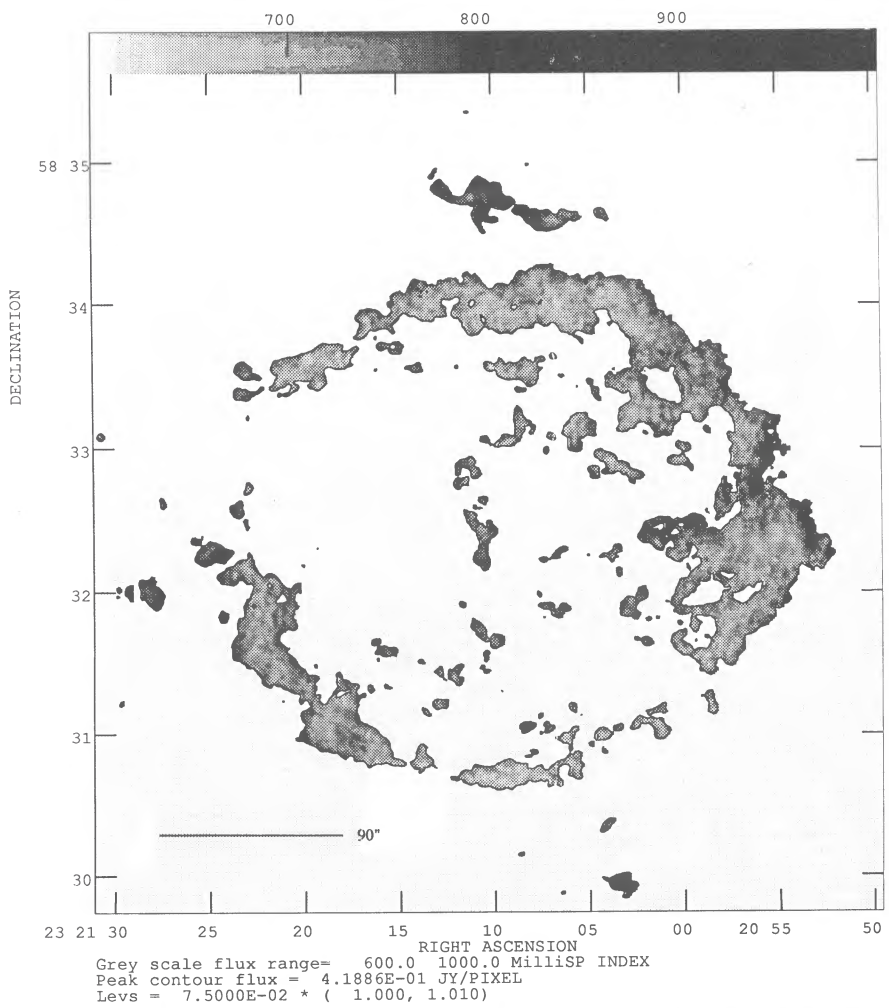

FIG. 3.—Spectral index distribution of Cas A between $\lambda 20$ cm and $\lambda 6$ cm, epoch 1987. The gray-scale range shown here represents a range in α between -1.0 and -0.6, the steeper regions being darker. Only pixels with corresponding L-band flux greater than 6 mJy pixel^{-1} are displayed. The bar represents a spatial scale of 90″—the largest scale sampled in our data.

with L-band flux density levels greater than 6 mJy pixel^{-1}. A discussion of errors inherent in this map is given in § 3.1. A description of the observed spectral variations is presented in § 3.4 and interpretations of these variations in § 4. Because structure in Cas A exists at a variety of spatial scales, and because the very largest of these scales are not well sampled in our data, it is important to verify that the variations we detect are not due solely to an extended background component which may or may not be correctly reconstructed in our maps. To this end we are experimenting with various spatial filters, which will effectively remove structures on scales larger than that of the radio ring. A comparison of the results from the filtered and unfiltered maps provides a means of determining the degree to which our spectral index measurements in small-scale features are being contaminated by the background. Our most successful filtering experiment to date is discussed in §§ 3.2 and 3.3.

We note again that the overall spectral index of Cas A is -0.77 ± 0.01 (Baars et al. 1977) and is observed to be flattening at a rate of $+0.00126 \pm 0.00023$ yr^{-1} (Dent et al. 1974). We detect reliable spatial variations in the spectra across Cas A (1987) in the range $-0.92 < \alpha < -0.64$. Significant fluctuations in spectral index are seen over angular scales ranging from $\sim 11''$ (~ 8 beams, 0.15 pc) to greater than 80″ (1.1 pc). We are sensitive to but do *not* detect significant variations on the scale size of our beam (1.″3, 0.02 pc). After filtering, the spectral index of small-scale features in the remnant varies from values steeper than ~ -1.1 up to ~ -0.46 (see § 3.2).

Readers should be aware that structure in Cas A exists over (and beyond) the entire range of spatial scales to which we were sensitive. Although the spectral indices themselves are reliable, their interpretation, whether using filtered or unfiltered maps, depends on assumptions made regarding what constitutes a physically separable component.

3.1. *Sources of Error in* α

The most significant limitation in our measurement of α is due to uncertainty in our reconstruction of the largest scale, low-surface brightness features. The shortest spacings were ≈ 0.5 kλ at both L ($\lambda 20$ cm) and C ($\lambda 6$ cm) bands. (The shortest L-band spacings available from the VLA D-configuration were eliminated to avoid problems due to the Van Vleck bias in the three-bit correlator.) Components greater than 90″ are therefore not completely sampled and may not be fully recon-

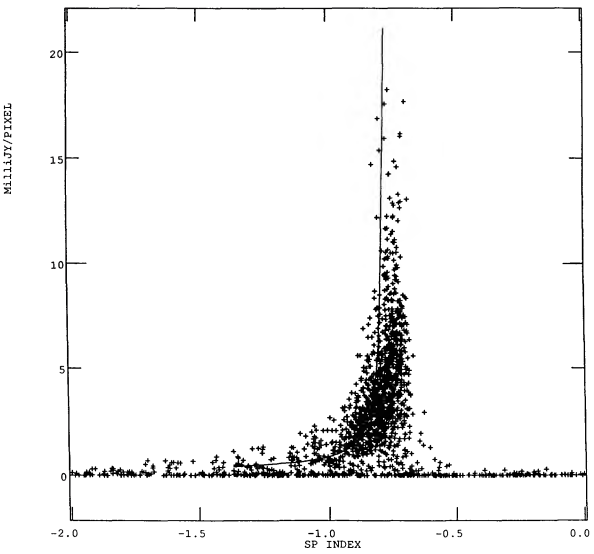

FIG. 4.—Scatter plot of brightness of Cas A (1987) at λ20 cm [flux (square 0".4 pixel)$^{-1}$] vs. spectral index. 1/225 of all pixels are plotted (~1 point per 5 beams). The solid line is an estimate of the bias from missing low-surface brightness flux, as discussed in the text.

structed in the maximum entropy maps. The expected flux, correcting for decay to epoch 1987 (Dent et al., 1974), is 1990 Jy at 1381 MHz and 751 Jy at 4970 MHz, whereas the maximum amplitudes of correlated flux contained on the shortest baselines in our data base were 1110 and 415 Jy. The maximum entropy procedure recovered 1948 and 717 Jy (missing ~67 Jy at L and 36 Jy at C), respectively.

This missing component is consistent with the observed bias toward steepness at low flux levels, as seen in the distribution of flux density at L band versus α (Fig. 4). To estimate the errors in spectral index due to missing flux, we have assumed that this flux is distributed in a similar and uniform way at both bands, over some fraction of the plateau. We then calculated the resultant bias in a set of pixels with an initial spectral index of −0.77. The curve overlaid on Figure 4 represents a best fit (by eye) to the distribution at low flux levels—it assumes the missing flux is concentrated in 1/3 of the plateau region. Given this curve, the calculated bias in α at 6 mJy pixel^{-1} is −0.03 and vanishes in the limit of high brightness. However, *the data show little or no bias above the level of 6 mJy pixel^{-1}, so we have adopted this to be the minimum flux cutoff in the following analysis.* We are currently investigating whether the observed large bias at low flux levels is intrinsic to the source, but this has no effect on the current analysis.

Spectral measurements can also be affected by a smearing of features due to motions during the annual cycle through the four VLA configurations. As an example of an extreme case, the fastest moving peaks in the maps have velocities of ~1.6 pixels yr^{-1}. The *A*-array component at L band was sampled approximately 0.25 yr before its *B*-array, *C*-band counterpart, which would yield a displacement of 0.4 pixels between observations. We tested for this problem by independently deriving peak fluxes at the two frequencies and then calculating the spectral indices, ignoring any small displacements. The results were in excellent agreement with spectral indices derived from our direct map division, so motions do not appear to be a significant limitation in our analysis. Furthermore, we see no evidence for fine-scale gradients from flat to steep in the direction of motion that would be expected from a motion-induced bias.

Despite problems with the background reconstruction (as discussed above), we have confidence that VTESS has done an accurate job of reconstructing the higher spatial frequency structures. The residuals of the VTESS reconstruction (the difference between the Fourier transform of the reconstructed map and the gridded UV data), in regions of the UV plane which were well sampled, are quite small. When transformed into the map plane, the flux densities of these residuals are between −0.30 and 0.05 mJy pixel^{-1} at L, and between −0.22 and 0.13 mJy pixel^{-1} at C. Figure 5 is a map of error in α, where Δα at a given pixel has been conservatively defined in terms of the quadrature sum of the observed residual flux at that pixel and the overall rms error in flux (0.04 mJy pixel^{-1} at L and C). Errors in regions above the cutoff level are less than ±0.045 in α and are typically ±0.015.

Other, more subtle problems, such as those due to combining data at several frequencies in each band (flux errors due to spatial variations in α, errors in correcting for the primary beam by assuming one nominal frequency, etc.), will also contribute to the maximum entropy residuals. The errors in α quoted above therefore reflect the actual uncertainties in comparing spectra between different locations on the map.

The exact values of spectral index quoted in this paper may contain a small bias (≈5%) due to errors in calibration; such a bias does not affect the variations in α discussed here.

3.2. *Spectral Index from Filtered Maps*

Before conclusions can be drawn concerning the distribution of spectral indices associated with the small- and intermediate-scale structure in Cas A, we must verify that our measurements are independent of the background upon which these compact features sit. If in filtering the extended structure from our maps we find a distribution in α similar to that in the unfiltered spectral map, we can be confident that we are measuring indices intrinsic to these smaller scales, and that the variations we detect are not spurious artifacts of the VTESS reconstruction of the poorly sampled short baselines. A map of spectral indices derived from filtered total intensity images is shown in Figure 6 for comparison with Figure 3.

Filtering short baselines from the UV plane prior to mapping led to a poor reconstruction of the remnant, as it truncated the Bessel function associated with the bright ring before its first zero. Thus it was necessary to experiment with filters which work on the map plane itself. The background removal algorithm used here subtracts a weighted average over all local minima within a radius of 12″ around each point. The weighting function is shown as an inset in Figure 7. This particular filter was chosen to give a smooth subtraction of angular scales greater than ~12″. The traces in Figures 7*a* and 7*b* slice through the entire remnant at a position angle of ~ −45°. Overlaid is the background subtracted by the filter at both frequencies. These traces show the level of errors committed by the filter and the spatial sizes to which it is sensitive. The filter introduces spurious rings around bright compact features with peak-to-peak errors of ~0.06 mJy in the C-band map and ~0.1 mJy in L. We chose a high clipping level (see below) to pass only the highest few peaks in this plot for spectral index determinations.

As evident in the distribution of filtered flux density versus spectral index (Fig. 8), the background filtering process has greatly reduced the bias toward steepening at low-surface

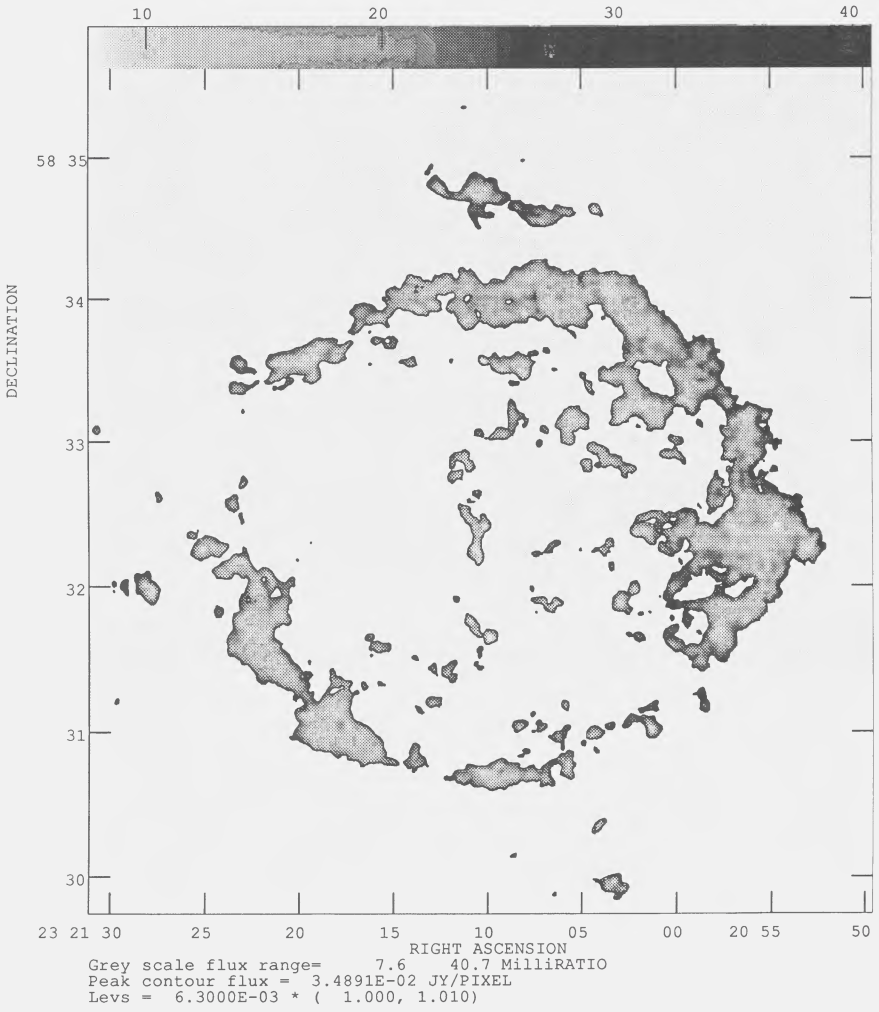

FIG. 5

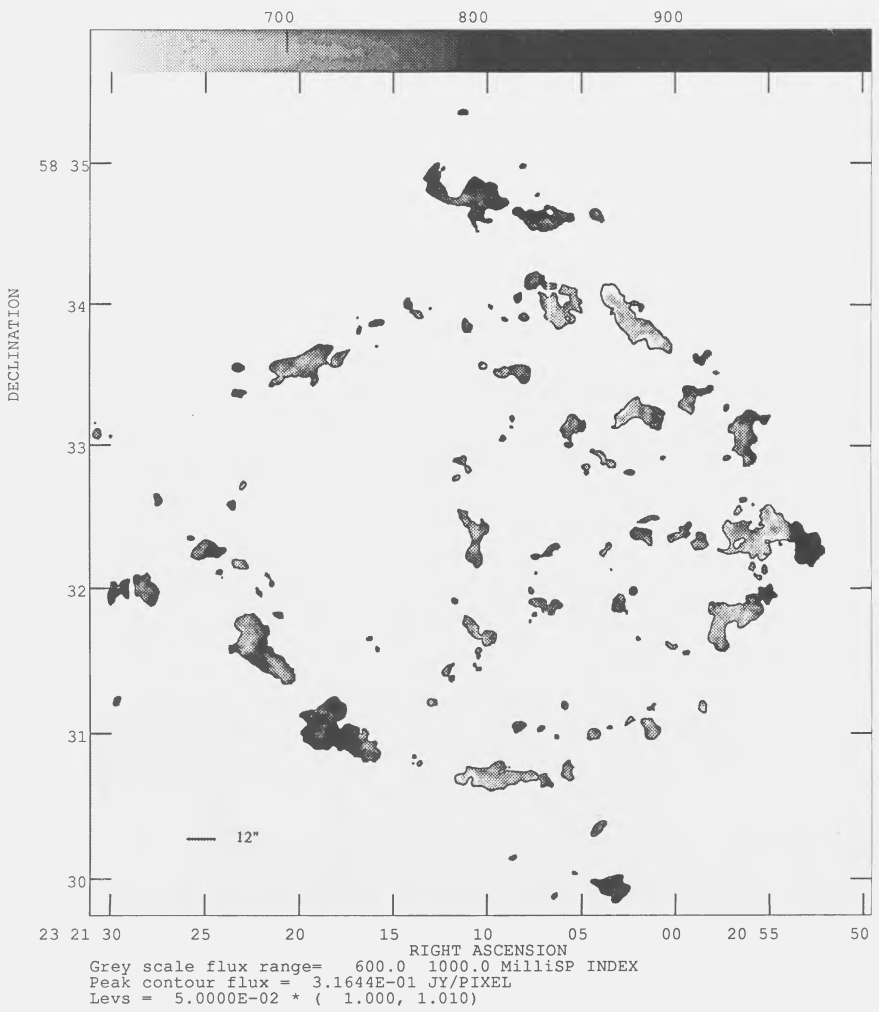

FIG. 6

FIG. 5.—Gray-scale map of errors in the spectral index measurements displayed in Fig. 3, as discussed in the text. Gray-scale range is 0–0.045. These propagated error estimates also incorporate the distribution of residual flux not well modeled by VTESS.

FIG. 6.—Spectral index distribution of Cas A between $\lambda 20$ cm and $\lambda 6$ cm, epoch 1987, using maps filtered to remove structure on scales $\geq 12''$ (length of bar). This image has been clipped below 4 mJy pixel^{-1}.

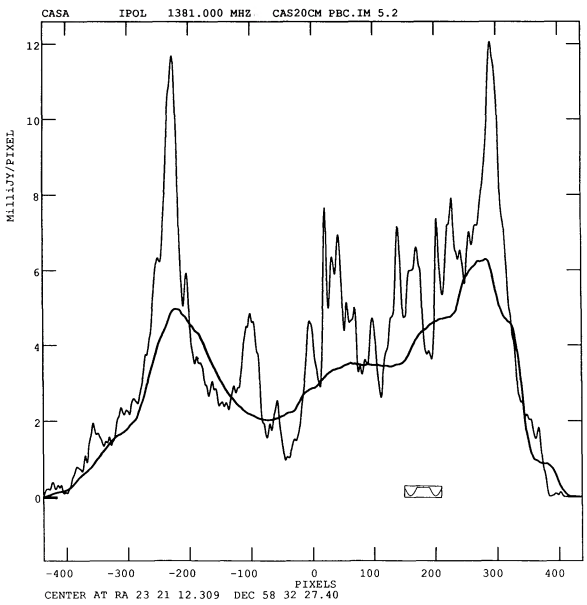

FIG. 7a

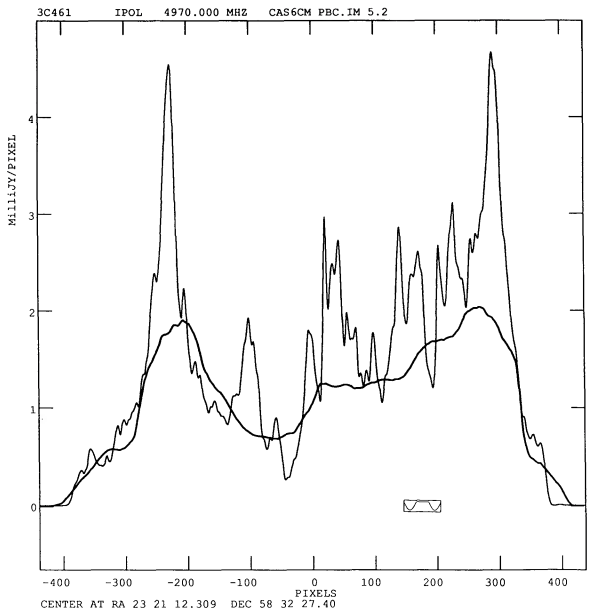

FIG. 7b

FIG. 7.—A slice from the unfiltered λ20 cm (*a*) and λ6 cm (*b*) maps, extending across the entire remnant. The bolder line represents the background determined along this axis by the spatial filter, shown to scale as an inset. We note that this experimental version of the filter creates some spurious spectral index values; the locations where the estimated background is *above* the actual data are the most obvious examples of these effects. See the text for a more detailed discussion.

brightness levels. The minimum flux cutoff level, based on this distribution, was chosen to be 4 mJy pixel^{-1}. The filtering has also widened the distribution, probably due to both the effects of noise and some small-scale intrinsic spectral variations which were masked by the background.

The spectral index distribution from the filtered maps shows the same general trends seen in the unfiltered maps. A typical rms difference between the two maps is 0.02, with some isolated regions, near very extended features, changed by up to 0.1 as a result of the filtering. The similarity between Figures 3 and 6 gives us confidence that our results are not significantly affected by background problems. We are currently developing a more refined filter which will allow us to use a lower clipping level.

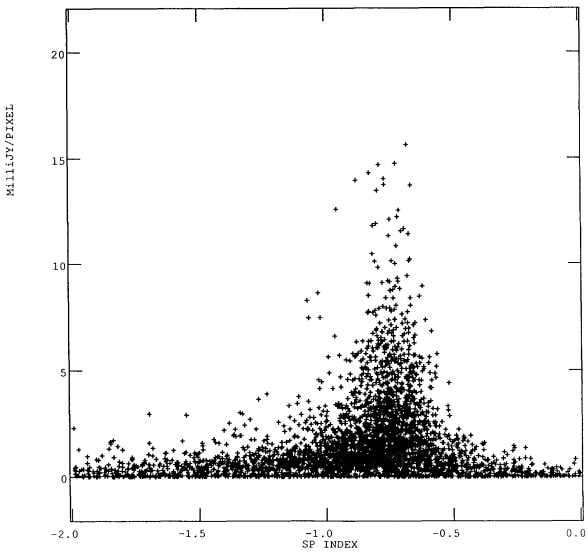

FIG. 8.—Scatter plot of brightness of Cas A (1987) at λ20 cm vs. spectral index, from the background filtered maps (as shown in Fig. 6). 1/144 of all pixels have been plotted (~1 point per 4 beams).

3.3. *Verification of α Variations*

As an independent means of verifying the existence of variations in α across the remnant, we have taken several slices through various features and derived spectral indices based on their peaks and apparent "background" levels. In doing so we, in effect, (a) eliminate errors due to displacement of peaks between the L- and C-band maps, and (b) isolate spectral indices of compact features from that of the larger scale background. We can compare these derived spectral indices with those from Figure 6 (filtered α) to evaluate the merit of our filters.

Shown in Figure 9 are two examples of slices, which represent the spectral extrema within the source. Subtraction of the underlying component in each case serves to amplify the diversity in α. Also shown are identical slices through the filtered L- and C-band maps. In each case the spectral index derived from the filtered peaks is very nearly equal to that derived through subtracting a local background from the unfiltered maps. These traces demonstrate the success of the filter at recovering true spectral indices of strong peaks which sit in regions of relatively uncomplicated background.

The width of the distribution in α, for features at a given flux density, above the cutoff levels (Figs. 4 and 8) gives a measure of the variations in spectral index present in our maps. One might ask, however, whether this width represents real fluctuations in α, or whether it is merely consistent with a flux^{-1} trend in the errors in α. Figure 10 shows a plot of rms variations in α within bins of constant L-band total intensity. Also plotted are two models of this rms distribution: the dotted line represents a pure noise distribution, fit to the measurements at low flux levels; the solid curve incorporates a constant, intrinsic rms

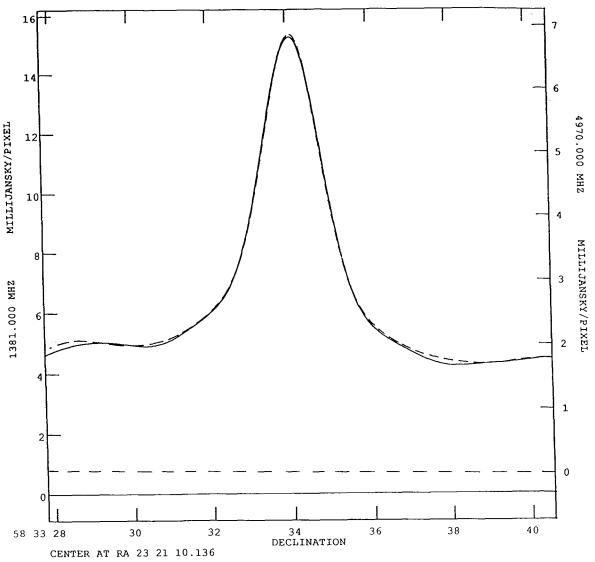

FIG. 9*a*

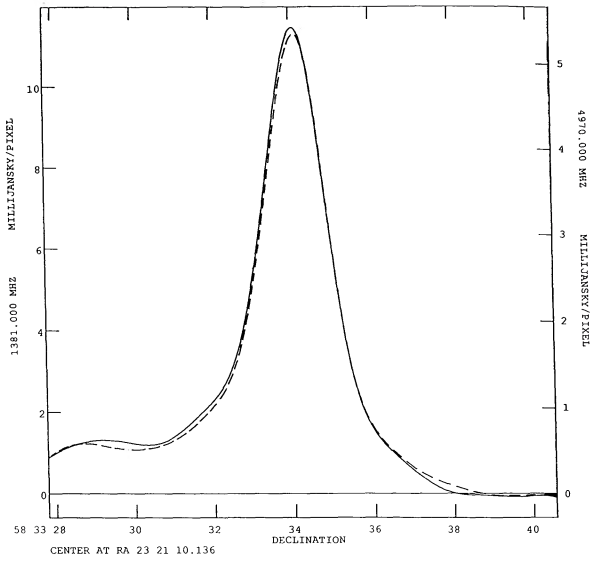

FIG. 9*b*

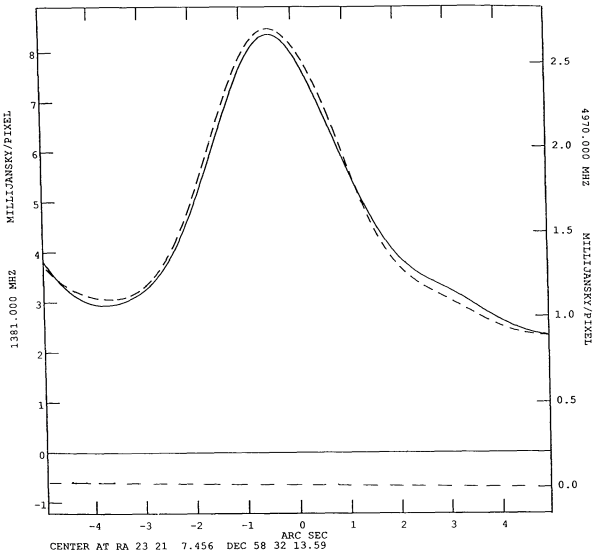

FIG. 9*c*

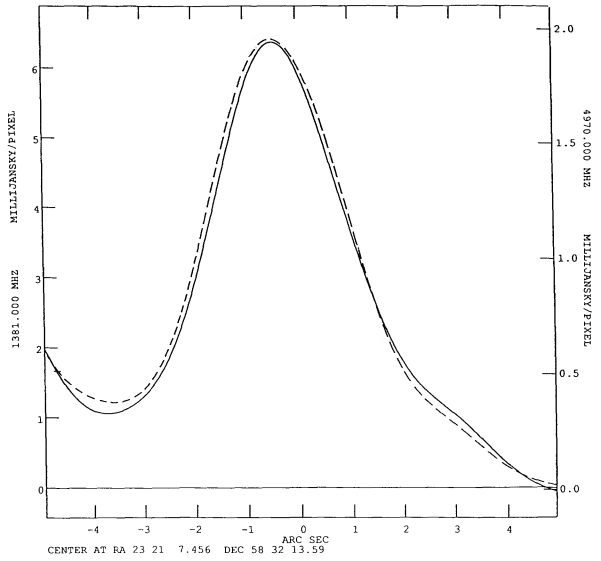

FIG. 9*d*

FIG. 9.—Slices through two strong peaks. Parts [(*a*) and (*c*)] and [(*b*) and (*d*)] are from the unfiltered and filtered maps, respectively. In each frame the dotted line and solid line represent the peak profile at $\lambda 6$ cm and $\lambda 20$ cm, respectively. Scales *and zero levels* have been adjusted such that the peaks coincide to emphasize the similarity at the two frequencies. Three spectral indices were determined for each peak—from the zero to peak levels, from a locally determined background (by hand) to peak level, and from the automatic filtering. The results, respectively, are as follows: 1st peak: −0.63 and −0.59 (*a*), −0.60 (*b*); 2d peak: −0.88 and −0.93 (*c*), −0.93 (*d*).

term of ± 0.03 in α, independent of flux density. (A solid line representing the rms in all sampled points greater than 15.5 mJy has been included.) The rms variations in spectra diverge from the pure noise estimate above ~ 3 mJy. Including an intrinsic rms term improves the fit to the data. At the level of our cutoff, the intrinsic variations and the pure noise term contribute equally to the overall rms. We therefore adopt the value 0.03 as characteristic of the real variations in α about the spectral mean, above and beyond fluctuations introduced by noise. Certain regions exhibit variations much larger than the overall rms (e.g., the bow shocks); however, these regions occupy a relatively small fraction of the map.

3.4. *Analysis of Spectral Variations*

Based on arguments presented in § 3.3, the maps in Figure 3 and, with some caveats, Figure 6 appear to represent real spectral index variations across Cas A. Several aspects of these maps may prove to be of physical importance.

The steepest regions in both the filtered and the unfiltered clipped spectral maps tend to be in compact features. This is directly opposite to the standard behavior in hot spots in radio galaxies, where high-emissivity regions are flat (≈ -0.5) and are expected to steepen with time by synchrotron losses. These issues will be discussed in greater depth in § 4. The low-level plateau in the unclipped map also appears steep, but the spec-

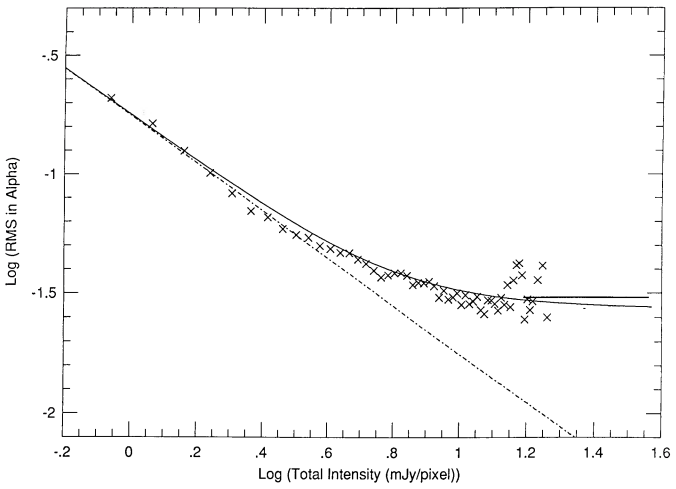

FIG. 10.—Crosses represent the rms in α determined in bins in total intensity, plotted on log-log scales. 1/9 of all pixels were sampled (~ 1 per beam) and only those bins which contain greater than 10 independent points are displayed. The solid bar designates the mean rms for all bins greater than 15.5 mJy. The dashed line is a model of pure 1/flux noise in α. The solid curve is given by $[(C/\text{flux})^2 + (0.03)^2]^{1/2}$, where C was determined by a fit to low flux levels, and the 0.03 term, by a fit to the high end. The measured rms values deviate from the pure noise model well below our chosen cutoff level.

tral index here cannot yet be trusted because of the bias at low brightnesses.

In general, the bow shocks, previously identified by BGP as regions of interest, also appear significantly steeper than other regions on the map. In fact, there are very few steep compact features which are *not* associated with a bow shock. The spectral indices of the bow shocks (those for which an index could be derived) and a typical point on the ring are plotted in Figure 11. Also plotted here, for comparison, are mean values of α over the entire remnant, determined within bins in L-band total intensity (*crosses*). The bias in the mean of α at low flux levels is clearly evident, but above our cutoff (6 mJy pixel^{-1}) it is less than -0.03. There does not appear to be any correlation between the brightness of a bow shock and its spectral index.

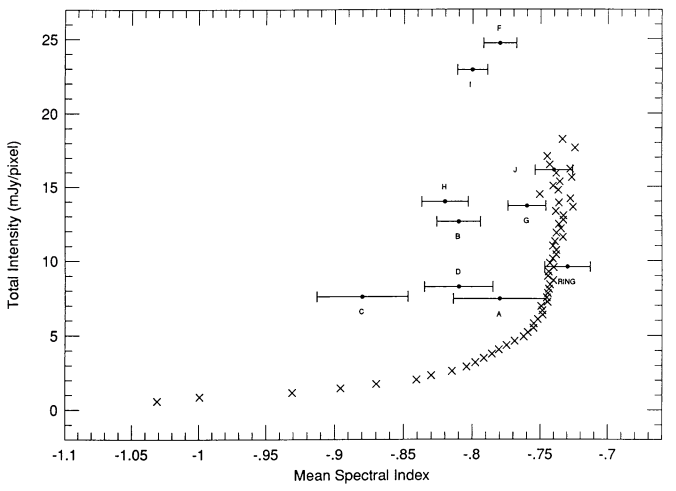

FIG. 11.—Crosses represent the mean spectral index determined in bins in total intensity. Also shown are points characterizing the mean spectral indices within the bow shock features and their associated errors. A point representing a typical spectral index and error found within the bright radio ring is included for comparison.

The radio ring is predominantly flatter than the overall average and shows a greater degree of spatial uniformity than other regions. The average spectral index in the ring is ~ -0.73, with significant fluctuations occurring on scales generally greater than or equal to 80″.

Spectral index appears to be relatively independent of brightness (above our flux cutoff); bright features are equally likely to be flat or steep. However, there does seem to be a correlation, for some features, between spectral index and rate of change in brightness. In comparing total intensity maps at epochs 1985 (BGP) and 1987, many of the steepest regions (including the bow shocks) appear to be brightening rapidly, while flatter regions (e.g., the ring) brighten or fade at a much slower rate. Over this two-year interval, several of the bow shocks increased in brightness by 5% to 12%, whereas the ring typically faded or brightened by only 1%. There are, however, exceptions to both trends, so the correlation must be interpreted with caution.

Little or no correlation has been found between α and velocity within a set of 300 pointlike features for which we have measured motions over five epochs. Residual velocities, calculated by subtracting a uniform expansion component from the observed velocities, similarly show no trend with the spectral index.

4. INTERPRETATION

The acceleration of relativistic particles is important in a number of astrophysical environments, from the production and resupply of galactic cosmic rays to the synchrotron emission from pulsars, supernovae, and their remnants, and from nuclear and extended radio galaxies and quasars. Several well-established arguments demonstrate the need for particle acceleration in supernova remnants: the "radio turn-on" of SNRs after 10^2 years in the face of continuing expansion losses, the observed spectral flattening with time of Cas A (Dent et al. 1974), and the need to find a sufficient energy source for galactic cosmic rays. Our observations of spectral index variations across Cas A provide important new information about particle acceleration processes in young SNRs.

It is first useful to note that the synchrotron emissivity in the compact features in Cas A ranges up to 10^9 times a typical interstellar value of $\approx 10^{-30}$ ergs cm^{-3} (see, e.g., Badhwar, Daniel, & Stephen 1977). This enormous increase cannot be realized simply by compression of the ISM. Nor can the original stellar ejecta contain the requisite relativistic particles and fields (e.g., Reynolds 1988a), or the emissivity of very young SNRs would be many orders of magnitude larger than observed (Weiler et al. 1986). We conclude, based on this and on other arguments presented below, that some form of particle acceleration must have occurred in or around Cas A.

Most theoretical work to date on particle acceleration in SNRs has centered around the first-order Fermi mechanism, as it is much more efficient than second-order, turbulent processes. We therefore begin, in §§ 4.1 and 4.2, by exploring a variety of scenarios and conditions in search of a simple first-order acceleration model which will explain, simultaneously, the high synchrotron emissivities, the spectral index variations, and the various types of structures that we observe in our radio maps of Cas A. It becomes readily apparent that no such simple model exists, at least in the test-particle limit for shock acceleration. Small pieces of the puzzle can be assembled, given a careful selection of assumptions, but we are unable to complete the picture. In § 4.3 we discuss briefly other acceleration mechanisms which can be considered.

4.1. *Spectral Variations and Shock Acceleration*

Our basic observational result is that the "bow shocks," as identified by BGP, typically have steeper spectral indices than the bright radio ring. We follow BGP's interpretation of these bow shocks as resulting from clumps of moderate density ejecta (as distinct from the high-density optical knots) which have penetrated the extended contact discontinuity region (i.e., the turbulent interface between the more diffuse ejecta and the ISM). The bow shocks are still within the region of diffuse X-ray emission mapped with the Einstein HRI (High Resolution Imager) by Fabian et al. (1980), and so we assume that they are currently encountering the already shocked ISM. We further assume that the ISM is the only important source of seed relativistic particles and fields.

In this model we have several possibilities for explaining the spectral variations within the remnant. At this point we assume that the cosmic ray pressure is small compared to that of the shocked thermal gas, so that the test particle limit applies for relativistic particle acceleration (see, e.g., Blandford & Eichler 1987). We first ask whether the relativistic particles can be accelerated rapidly enough to reflect dynamical changes which are occurring in the remnant. A fiducial time scale, τ_0, may be calculated using (both upstream and downstream) the standard Bohm diffusion coefficient $\kappa_{\rm Bohm} = r_g v/3$, where r_g is the gyroradius of the electrons and v is their velocity ($\approx c$). For a parallel shock, this leads to:

$$\tau_0 = (3\kappa_{\rm Bohm}/\delta U)(1/U_1 + 1/U_2) ,$$

where $U_{1,2}$ are the upstream and downstream velocities, and δU is their difference. Using $4U_2 = U_1 \sim 10^{3.5}$ km s^{-1} and an equipartition field of 4 mG (see § 4.2 for justification) yields $\tau_0 \approx 10^2$ s. There is considerable uncertainty about these estimates; it is possible that parallel shock scattering occurs only on much longer length scales, which would increase τ_0. On the other hand, Jokipii (1987) has argued that the perpendicular scattering scale can effectively decrease, leading to much faster acceleration times. In any case, it appears that the particle acceleration is happening on scales much faster than the $\approx 10^8$ s time scales over which dynamical changes occur in the remnant.

In this test particle approximation, we therefore assume that the spectral index will achieve its equilibrium value, $\alpha = 3/[2(r-1)]$, where r is the outer shock compression ratio. In terms of the Mach number (M) for a $\gamma = 5/3$ gas,

$$\alpha = [M^2 + 3]/[2\,(M^2 - 1)] .$$

One possibility then is that the relativistic electrons are Fermi-accelerated at the outer shock, and subsequently compressed by fast-moving clumps of ejecta to produce the bright ring and the bow shocks. As the outer shock gets weaker and decelerates, it produces progressively steeper spectra, so that the older (left behind) particles in the bright radio ring would be flatter than the bow shocks, as observed. To give spectra of ≈ 0.65 (≈ 0.85) in the ring (bow shocks) requires Mach numbers of ≈ 3.8 (2.6). These values create a problem, because it is unlikely that the outer shock has such low Mach numbers at this point in the remnant's evolution; the observed post-shock X-ray temperatures of 3×10^7 K (Jansen et al.) would require an unrealistic external temperature of $\sim 10^7$ K to get the Mach numbers sufficiently low.

Another possibility is that the outer shock heats the thermal gas and sets up the conditions for magnetic field amplification (see below), but does no more than compress the relativistic particles from the ISM. Then the clumps of ejecta create bow shocks as they penetrate the contact discontinuity and accelerate these relativistic particles. If the clumps of ejecta have some characteristic velocity, then they would have higher Mach numbers at the bright radio ring, where the X-ray temperature is observed to be lower than in the region of the isolated bow shocks, where the X-ray temperature is higher. The difference in local Mach numbers then could lead to the observed spectral differences.[3]

We can compare the Mach numbers of the bow shocks derived from their shapes with the shock speeds determined by Braun (1987) from the dust, radio, and X-ray emission of Cas A. For example, we assume that bow shock C of BGP (the extreme north point) was created while the ejected material was still at its initial velocity of 5700 km s^{-1}, before being decelerated to the observed proper motion velocity of 4500 km s^{-1}. If the outer shock in the north is advancing at 3100 km s^{-1}, as suggested by Braun, then the relative motion of a bow shock in the post–outer shock fluid would result in a Mach number of approximately 1.4. BGP derive a Mach number of 2.3 for bow shock C, based on its opening angle. These values are in good agreement and also very close to those derived above from the equilibrium spectral index.

Our conclusion regarding the spectral index variations is that the model of bow shocks penetrating into previously shocked material appears promising, although it currently relies on our assumptions about the ejectum velocity and we have not, as yet, made any demands for high emissivities (see next section). While such a model should allow us to predict the spectral indices of the bow shocks from their Mach numbers, no direct Mach number–spectral index relation is yet observed.

4.2. *Energetics and Shock Acceleration*

We now turn our attention to the *energetics* of the relativistic particle acceleration. The enormous energy stored in the radio-emitting plasma (greater than 5×10^{49} ergs in the ring alone)[4] is already uncomfortably close to Braun's (1987) estimate of 1.5×10^{50} ergs in the kinetic energy of the diffuse ejecta of Cas A. This tells us that conditions in Cas A must be very close to their minimum energy (or equipartition) values. Departures of the magnetic field from its minimum energy value ($H_{\rm min}$) would result in an increase of total energy of

$$(E/E_{\rm min}) \propto (H_{\rm min}/H)^{3/2} \quad (\text{for } H \ll H_{\rm min}) ,$$

or

$$(E/E_{\rm min}) \propto (H_{\rm min}/H)^{-2} \quad (\text{for } H \gg H_{\rm min}) .$$

Therefore, we use the minimum energy estimates for magnetic field values, which give 4 (14) mG for the bow shocks, assuming a proton-to-electron energy density ratio of 1 (or 100, as in cosmic rays). If we start with an average galactic field of 3 μG, then we cannot use shock compression to give us the required increase in field strength of up to 1300 (4700). Even if our bow

[3] The Mach numbers inferred by BPG from the shape of the isolated bow shocks range from ≈ 2–5, spanning the values required, although we could not detect a direct correlation between M and α.

[4] This minimum energy calculation assumes that the ring can be modeled by a shell of radius 107″ and thickness 17″ at a distance of 3 kpc. We use a proton-to-electron energy density ratio of 1 (although much higher ratios can be reasonably expected), which yields an average magnetic field of 1.6×10^{-3} in the ring.

shocks are located just behind the (unseen) outer shock, so that they can recompress (by a factor of up to 4) the already compressed interstellar field, we are still 2–3 orders of magnitude short of the required increase.

Gull (1973) suggested a plausible mechanism for amplifying the magnetic fields in the decelerating, Rayleigh-Taylor–unstable, contact discontinuity region. In this situation, the field also becomes radial, as observed in most young SNRs (Milne 1988) including Cas A. Gull's model has been extended by Dickel et al. (1989), who show how the instabilities depend on the clumpy nature of the external medium. In our attempt to account for the 10^9 increase in synchrotron emissivity, we will therefore assume that the material being encountered by the bow shocks has been field amplified by this or similar processes to the $\approx$mG minimum energy values.

Turning now to the relativistic particles, we start by assuming that the magnetic field amplification had no effect on their energy distribution (but see below). If we start with the observed cosmic ray electron flux of 367 $E^{-3.15\pm0.2}$ electrons m^{-2} sr^{-1} s^{-1} Gev^{-1} (Golden et al. 1984), and simply put them in a magnetic field of 4 (14) mG,[5] we find ourselves a factor of 10^5 (10^6) too low in synchrotron emissivity. Adiabatic compression of the galactic cosmic ray electrons could contribute up to a factor of ≈ 10 (4 for compression in density and the rest from integrating a $4^{1/3}$ increase in energy per particle). This still leaves us a factor of 10^3 (10^4) too low in emissivity. Thus, direct acceleration of the relativistic particles seems necessary.

Another indication of the need for particle acceleration comes from the spectrum of the galactic nonthermal background emission (as suggested to us by S. Reynolds). Below $\approx$400 MHz (see review by Salter & Brown 1988) the spectral index of the galactic background flattens to ≈ -0.5, then turns over at $\approx$2–3 MHz due to thermal absorption. With magnetic fields approximately 10^3 times higher than in the ISM, Cas A's radiation at 5 GHz would be from the same electrons radiating in the ISM at 5 MHz. Note that since the integrated spectrum of Cas A is much steeper than -0.5, we must account for a net steepening of the seed population by >0.2 over a time scale of 300 years. Neither synchrotron losses nor particle acceleration can account for this. However, if the particle acceleration mechanism uses seed particles from energies below those radiating at the 2–3 MHz turnover, then we do not have a direct measure of their spectrum. In order to explain the integrated spectrum of Cas A with particle accleration of ISM electrons, we would therefore need to invoke a new, low-energy component to the cosmic ray electrons. An extrapolation of the electrons radiating at less than 400 MHz in the ISM, with a spectral index of -0.5, *cannot* be used as the seed population.

We can see how far we can go toward explaining the high observed emissivities by relaxing the condition of low-Mach number expansion, inferred by the shapes of the bow shock features. If high values of M are acceptable, then perhaps a physical model can be constructed in which the radio features need not expand into a preshocked medium. If Cas A is expanding at speeds of 2300–3800 km s^{-1}, as suggested by Braun (1987), into a 5000 K medium, then Mach numbers of 200–300 would exist. These Mach numbers are within a factor of a few of those required to increase the pressures in relativistic particles from typical cosmic ray values (≈ 1 ev cm^{-3}) up to the minimum particle pressures measured in the bow shocks ($\approx 4 \times 10^5$ times higher for $k = 1$, 4×10^6 times for $k = 100$). This can be seen by looking at the mean gain in momentum per particle for shock acceleration in the steady state test particle limit, as derived by Blandford & Eichler (1987, following eq. [4.26]). From this we can find that the total required gain in momentum (equal to the gain in pressure, in the relativistic limit) can be achieved with $M = 800$ (1400).

If high Mach numbers are allowed, then it may be possible to produce the high emissivities observed in Cas A with first-order acceleration in the test particle limit. However, there are several serious objections to this picture. First, such high Mach numbers should lead to a spectral index of -0.5, much flatter than observed. Second, we must come up with alternative explanations for the shapes of the "bow shock" features. Third, the minimum pressures in relativistic particles and fields are each $\approx 1/4$ of the X-ray pressures, which suggests that a large fraction of the shock energy goes into these components. In that case, the shock will be broadened, and the test particle limit will no longer apply. More detailed modeling of Cas A using cosmic ray–mediated shocks is therefore necessary. Mixed shocks have the added attraction in the case of Cas A that they can produce steeper spectra than simple one-fluid models (see, e.g., Blandford 1980).

4.3. *Turbulent Acceleration*

Our discussion above has examined how far one could explain the observations of Cas A using first-order acceleration at shocks with small cosmic ray pressures. We find that a fully self-consistent picture cannot be built. The existence of radial magnetic fields and other difficulties in the above analysis suggest that turbulent particle acceleration, a second-order process, is also important. Such a proposal for Cas A was first made by Scott & Chevalier (1975) and later developed in more detail by Cowsik & Sarkar (1984). The latter authors described the evolution of the spectral index toward flatter values, even as adiabatic losses resulted in a drop in luminosity. Such a behavior is reflected in the comparison between the (probably) younger steep spectrum bow shocks and the fading, but flat spectrum bright ring.[6] Acceleration via turbulence is also included in the clumpy medium models of Dickel et al. (1989).

None of the calulations of turbulent particle acceleration explicitly includes the concomitant amplification of the magnetic field. This could well result in an energy transfer process similar to the betatron mechanism and might be of primary importance for Cas A and other supernova remnants.

The importance of the results presented here is that they offer the opportunity to link the dynamical behavior of the remnant with the particle acceleration processes. Future work will include a more detailed investigation of the dynamics as well as an attempt to measure the time evolution of the local spectra.

5. CONCLUSIONS

1. We observe spatial variations in the λ20 cm/λ6 cm spectral index distribution in Cas A in the range between -0.92 and -0.64. The variations occur on scales of 0.15 pc to greater

[5] In 4 mG equipartition fields we are sampling particle energies of 150 and 270 Mev at L and C bands, respectively.

[6] This flattening of the spectral index with time is *opposite* to that which is inferred for larger scale synchrotron sources, such as radio galaxies and quasars. There, the spectra steepen through synchrotron and/or inverse Compton losses. In Cas A, the shortest lifetimes to synchrotron losses are $\approx 10^4$ yr in a field of $\approx$4 mG, and are therefore not important.

than 1.1 pc but are *not* seen down to our limiting resolution of 0.02 pc. We have tested the reality of these variations for a variety of instrumental and other effects.

2. The steepest regions tend to be compact features, especially the bow shock regions identified by their morphology and polarization behavior. The compact nature of the bow shocks and their rapid evolution in structure and brightness suggest that these are young features. Flatter spectral regions tend to be associated with the bright radio ring. These results indicate a direct link between the dynamics of the remnant and the distribution of relativistic electrons.

3. We observe a relation between the spectral index of some features and their change in brightness between 1985 and 1987. There is wide variation in behavior, but many of the steepest features are found to be brightening rapidly, while flatter regions tend to change in brightness at a much slower rate.

4. We examined the spatial variations in spectra and the energetics of models invoking relativistic particle acceleration at shocks. We find that models based on first-order acceleration processes in the test particle limit can be constructed which are consistent with the apparent spectral variations, or with the high emissivities observed within certain compact features, but not with both, simultaneously.

5. The failure of the simplest models presented here requires that models be developed for Cas A involving other types of mechanisms, including mediated shocks and turbulent acceleration with secularly increasing fields.

This work was supported, in part, by NSF grant AST 87-15949 at the University of Minnesota, and by a grant of computing time from the Minnesota Supercomputer Institute. We are grateful for discussions early in this project with R. Blandford and S. Reynolds, and for the continuing advice of T. W. Jones. S. Reynolds served as the critical and very helpful referee. Our thanks also to Eric O'Dell and Brian Neurauter for countless hours of staring at blobs on the screen.

REFERENCES

Altenhoff, W., Downes, D., Pauls, T., & Schraml, J. 1978, A&AS, 35, 23
Baars, J. W. M., Genzel, R., Pauliny-Toth, I. I. K., & Witzel, A. 1977, A&A, 61, 99
Badhwar, G. D., Daniel, R. R., & Stephen, S. A. 1977, Nature, 365, 424
Blandford, R. 1980, ApJ, 238, 410
Blandford, R., & Eichler, D. 1987, Phys. Rept., 154, 1
Braun, R. 1987, A&A, 171, 233
Braun, R., Gull, S. F., & Perley, R. A. 1987, Nature, 327, 395 (BGP)
Bridle, A. H. 1967, MNRAS, 136, 219
Cowsik, R., & Sarkar, S. 1984, MNRAS, 207, 745
Dent, W. A., Aller, H. D., & Olsen, E. T. 1974, ApJ, 188, L11
Dickel, J. R., Eilek, J. A., Jones, E. M., & Reynolds, S. P. 1989, ApJS, 70, 497
Fabian A. C., Willingale, R., Pye, J. P., Murray, S. S., & Fabiano, G. 1980, MNRAS, 193, 175
Golden, R. L., Mauger, B. G., Badhwar, G. D., Daniel, R. R., Lacy, J. L., Stephens, S. A., & Zipse, J. E. 1984, ApJ, 287, 622
Green, D. A. 1988, in Genesis and Propagation of Cosmic Rays, ed. M. M. Shapiro & J. P. Wefel (Dordrecht: Reidel), 205
Gull, S. F. 1973, MNRAS, 161, 47
———. 1975, MNRAS, 171, 263
Jansen, F., Smith, A., Bleeker, J. A. M., de Korte, P. A. J., Peacock, A., & White, N. E. 1988, ApJ, 331, 949
Jokipii, J. R. 1987, ApJ, 313, 842
Klein, U., Emerson, D. T., Haslam, C. G. T., & Salter, C. J. 1979, A&A, 76, 120
Mauche, C. W., & Gorenstein, P. 1989, ApJ, 336, 843
Milne, D. K. 1988, in IAU Colloq. 101, The Interaction of Supernova Remnants with the Interstellar Medium, ed. R. S. Roger & T. L. Landecker (Cambridge: Cambridge University Press), 351
Minkowski, R. 1959, in Paris Symposium on Radio Astronomy, ed. R. N. Bracewell (Palo Alto: Stanford University Press), 315
Reynolds, S. P. 1988a, in Galactic and Extragalactic Radio Astronomy, ed. G. L. Verschuur & K. Kellermann (Berlin: Springer), 439
———. 1988b, ApJ, 327, 853
Rosenberg, I. 1970, MNRAS, 151, 109
Salter, C. J., & Brown, R. L. 1988, in Galactic and Extragalactic Radio Astronomy, ed. G. L. Verschuur & K. Kellermann (Berlin: Springer), 1
Scott, J. S., & Chevalier, R. A. 1975, ApJ, 197, L5
Sironi, G. 1974, MNRAS, 166, 345
Stewart, G. C., Fabian, A. C., & Seward, F. D. 1983, in Supernova Remnants and Their X-Ray Emission, ed. J. Danziger & P. Gorenstein (Dordrecht: Reidel), 59
Thompson, A. R., Clark, B. G., Wade, C. M., & Napier, P. J. 1980, ApJS, 44, 151
Tuffs, R. J. 1986, MNRAS, 219, 13
van den Bergh, S., & Dodd, W. W. 1970, ApJ, 162, 485
Webster, A. S. 1974, MNRAS, 166, 355
Weiler, K. W., Sramek, R. A., Panagia, N., van der Hulst, J. M., & Salvati, M. 1986, ApJ, 301, 790
Woan, G., & Duffett-Smith, P. J. 1990, MNRAS, 243, 87